

*Research Article*

## Three-dimensional connectivity in the Gulf of California: an online interactive webpage

Carolina Montaña-Cortés<sup>1</sup>, Silvio G. Marinone<sup>1</sup> & Ernesto Valenzuela<sup>1</sup>

<sup>1</sup>Department of Physical Oceanography, Ensenada Center of Scientific Research and Higher Education (CICESE), Tijuana, Mexico

Corresponding author: Silvio G. Marinone (marinone@cicese.mx)

**ABSTRACT.** This paper presents an online interactive webpage [<http://connectivity-dispersion.cicese.mx/>] that provides users with results of both the three-dimensional connectivity and spatial dispersion of particles in the Gulf of California (GC). These results were originated by means of a three-dimensional numerical model of circulation adapted to the GC from which the advection of particles were generated between different regions of the gulf. Particle connectivity and dispersion results were generated for and are limited to temporal scales to seasonal tides, which may aid in the interpretation of larval connectivity and contaminants within the gulf.

**Keywords:** interactive webpage, three-dimensional connectivity, particles dispersion, Gulf of California.

### INTRODUCTION

Three-dimensional connectivity studies are an important research topic for the different branches of oceanography because they provide information about the location of moving particles based on the hydrodynamics of a water body.

This study considers connectivity to be that which “connects” different areas to different times, describing some type of trajectory. These trajectories can serve as the basis for understanding contaminant propagation and the dispersion of larvae from different marine species and their nutrients and can aid in the sound development of protected marine areas, among other applications (Cudney-Bueno *et al.*, 2009; Marinone *et al.*, 2008).

The objective of this study is to demonstrate the manner in which an interactive online webpage [<http://conectividad-dispersion.cicese.mx/>] displays the evolution of three-dimensional connectivity between the areas composing the Gulf of California (GC), as well as to present a visualization of the dispersion of particles from a particular region based on the results obtained through the Hamburg Shelf Ocean Model (HAMSOM), which is an Eulerian numerical circulation model, and a Lagrangian particle dispersion model. Both models were validated as described in the following section.

### MATERIALS AND METHODS

Particles underwent advection for eight weeks, being released the first day of each month of the year through a Lagrangian advection-diffusion model (Visser, 1997; Proehl *et al.*, 2005) over a field of Eulerian currents obtained from a three-dimensional baroclinic circulation model (HAMSOM) adapted to the GC by Marinone (2003, 2008). The model has a spatial horizontal resolution of  $\sim 1.3 \times 1.5$  km and 12 layers vertically, and is forced by tides, winds, seasonal warming and water flows at the surface, and seasonal hydrography at the mouth of the gulf (Marinone 2003, 2006, 2008; Marinone & Lavín, 2005; Santiago-García *et al.*, 2014; Montaña, 2015). Given this forcing, there is no interannual or mesoscale variability beyond that which is obtained from nonlinear interactions between the currents produced by tides and seasonal currents produced by wind and forcing at the mouth. In particular, at these scales, the trajectories of particles are dominated by seasonal circulation, and tides only produce oscillations along the length of a trajectory (Marinone *et al.*, 2008). For calculations, at different scales, forcing in the numerical model will need to be changed to produce circulation during, for example, an El Niño event.

The particles release was performed within the 17 areas into which the Gulf of California was divided

**Table 1.** Names of the regions that correspond to the Gulf of California (Santiago-García *et al.*, 2014). Names are shown in both Spanish and English, as the webpage includes both options.

Acronym	English	Spanish name
UG	Upper Gulf	Alto Golfo
BZ	Buffer Zone	Conexión Alto Golfo y Remolino Estacional
PE	Peninsular Eddies	Remolinos Peninsulares
SE	Seasonal Eddy	Remolino Estacional
SO	Sonora Coast	Sonora
DB	Delfin Basin	Cuenca Delfin
TI	North of Tiburón Island	Norte de Isla Tiburón
AG	East of Ángel de la Guarda Island	Ángel de la Guarda
BC	Ballenas-Salsipuedes Channel	Canal de Ballenas
SZ	Sills Zone	Zona de los Umbrales
CP	Central Peninsular Region	Región Peninsular Central
GB	Guaymas Basin	Cuenca Guaymas
CC	Central Continental Region	Región Continental Central
SC	South Continental Region	Región Continental Sur
FB	Farallón Basin	Cuenca Farallón
SP	South Peninsular Region	Región Peninsular Sur
PB	La Paz Bay	Bahía la Paz

(Table 1; according to Santiago-García *et al.*, 2014). The final positions of the particles were determined (longitude, latitude and depth) at 2, 4, 6 and 8 weeks after being released. Then, the results were presented in connectivity matrices between the different areas, including the average depths and standard deviation, as well as in final position maps of all the particles and histograms of the percentage of particles corresponding to the different areas of arrival, as subsequently explained.

The connectivity matrices quantify the particles that reached different regions and those that returned or remained in the area where they were released for each of the final periods (2, 4, 6 and 8 weeks), shown as percentages. For each connectivity matrix,  $C_{ij}(t)$ ,  $i$  is the horizontal axis, which defines the area of arrival or final destination of the particles,  $j$  is the vertical axis, which represents the provinces or release areas, and  $t$  is the week at which the positions of released particles are observed during the different months of the year. The summation of the percentages in each of the rows of the matrix represents the total release percentage of each area, except when the particles leave the model domain. (In the connectivity figures, cells with less than 5% of the particles were excluded from the matrices for clarity purposes).

Associated to the connectivity matrices, the mean and standard deviation of the depths reached by the particles for each of the different cells of the matrix were calculated. Based on the information attained, matrices were developed for mean depth and standard deviation, which maintain the same format as the connectivity matrix. The sequence of matrices is such

that both the abscissa (x) and ordinate (y) axes group the regions as north, large islands and south. These divisions are presented in the figures as dashed lines. The principal diagonal line represents the retention and indicates the particles that ended up inside the release area.

To complement the portrayal of the connectivity results, mean depth, and standard deviation matrices, maps were developed of the final geographic position of the particles at different times (2, 4, 6 and 8 weeks), presented as color codes of depth at which each particle was found. Similarly, histograms were used to represent the connectivity percentages of a location compared to all other regional divisions that compose the GC. Therefore, for the model's 12 layers, the results represent all months of the year as well as the periods of 2, 4, 6 and 8 weeks.

## RESULTS

### Model validation

The results obtained using the Eulerian and Lagrangian models upon which the calculations presented for this webpage are based have been validated in several studies. The Eulerian model used by Marinone (2003) reproduces several circulation phenomena from the GC. For example, it adequately reproduces seasonal circulation patterns, which consist of a reversible rotation in the northern GC (NGC) that is anticyclonic in the winter and cyclonic in the summer, as reported by Lavín *et al.* (1997) and Carrillo *et al.* (2002), and a similar circulation pattern in the southern part of the

GC, as noted by Beier (1997). Similarly, Marinone (2008) validates the numerical results of the deep circulation present around the large islands obtained by López *et al.* (2006), which consisted of a trajectory from Umbral de San Esteban to the northern end of the channel formed between Ángel de la Guarda Island and the Baja California Peninsula (Ballenas-Salsipuedes Channel, or BC), exhibiting convergence in deep areas and divergence on the surface.

The tidal currents (barotropic and baroclinic), and their harmonic components reproduced by the model, exhibited similar behaviors with respect to the data obtained by Marinone & Lavín (2005). The numerical results were compared with 124 time series corresponding to 62 stations, of which 68 time series correspond to NGC, 31 correspond to the region of large islands and 25 correspond to the central gulf. A comparison indicates that the semidiurnal components were better modeled than the diurnal components. For example, in Table 2 from Marinone & Lavín (2005), the semi-major axis of the modeled M2 exhibits an underestimation of only 3.9%, whereas the underestimation for K1 is 26%. However, as mentioned in the study, when examining the means of the semi-major axis values together with their corresponding error bars, there is markedly a high number of overlapping data points, indicating better modeling than what is indicated by the significant differences. The numerical results obtained for sea level were validated with respect to the observations of Ripa (1990) and Beier (1997). The mean amplitude of the annual component in the coastal stations was  $18.8 \pm 4.5$  cm for the model, whereas it was  $18.6 \pm 4.5$  for the observations (Marinone, 2003). The comparison of sea surface temperatures obtained from the model with sea surface temperatures obtained from the region studied by Soto-Mardones *et al.* (1999) revealed that the evolution of warm and cold water pools was reproduced in the central part of the NGC, as well as the presence of a lateral temperature gradient during the summer in the southern part of the GC (Marinone, 2003). For further validation of the currents obtained by the model, refer to [<http://gulfcac.cicese.mx/>].

The Lagrangian behavior obtained from particle advection was also validated by comparing the results obtained for the trajectories of buoys (ARGOS) released in the NGC in September (1995) and March (1996) by Lavín *et al.* (1997), where one cyclonic and one anticyclonic rotation were observed. Additionally, Calderon-Aguilera *et al.* (2003) described the migratory patterns of the blue shrimp by associating the circulation patterns during the summer in the northern part of the GC. In that study, every day and during two periods (July 12–27, 1995 and June 30 to July 16,

1996), simultaneous samples of post-larval shrimp were collected in two locations of the NGC (San Felipe on the peninsula side, and Santa Clara on the continental side of the GC). To simulate circulation, the output of the HAMSOM model was used. From the significant results, it was determined that the model served as an important tool to explain why the post larvae found in the continental sector were bigger (apparently, they were older) than those found on the peninsula side. Similarly, Cudney-Bueno *et al.* (2009) used this model to evaluate the possible effects of the reserve network of the upper gulf's continental sector on adjacent areas. The results of the model were compared with oceanographic experiments and the changes observed in the density of commercial juvenile mollusks before and after establishing the reserves. In that respect, the model suggested that San Jorge Island, on the southern side, in particular, could be responsible for exporting larvae to the reserves and fishing areas along the coast. Munguia-Vega *et al.* (2014) hypothesized that the source-sink metapopulation dynamic of the *Mycteroperca rosacea* larvae in 17 zones distributed across the Great Islands describes the direction and frequency of larval dispersion based on an oceanographic model (HAMSOM) that favors the understanding of empirical genetic data.

The comparison of model results (Eulerian and Lagrangian), with the described observations reported in the different studies cited, lends qualitative confidence to using this online tool to examine connectivity matrices and dispersion patterns throughout a climatological year.

### Webpage

The webpage [<http://conectividad-dispersion.cicese.mx/>] presents results for connectivity, dispersion, etc. both in English and Spanish. The page content was divided into four sections: the first (Start) provides a brief explanation of the methodology of products obtained as well as visualization options for the results presented in the second section (Interactive Map). The third section (Help) provides a brief explanation of how to use the webpage as well as some concepts, and the fourth section (Contacts) acknowledges collaborators involved in developing the page.

### Interactive map

In this section (Fig. 1), the user can select:

- Matrix – Connectivity matrices for mean depth and standard deviation
- Dispersion – Maps of final particle positions and histograms

To display the figures, one must first select the type of graph: matrix or dispersion. This option is located in

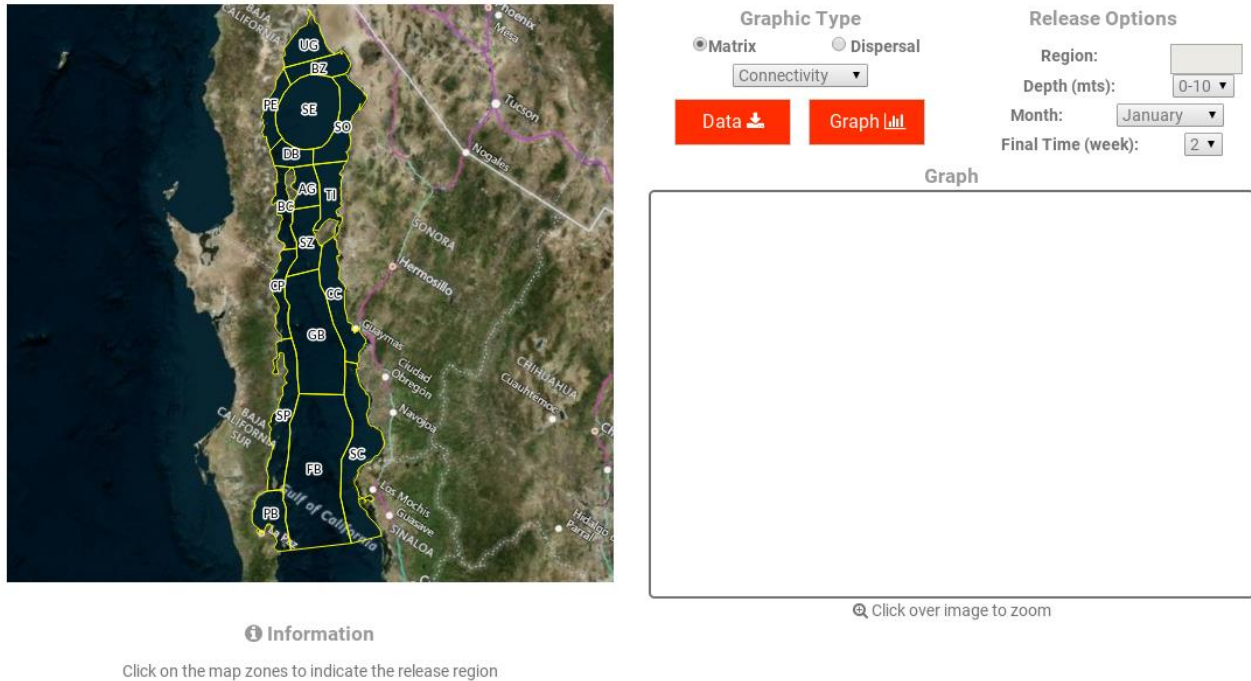


**Figure 1.** Image of the webpage’s interactive map section.

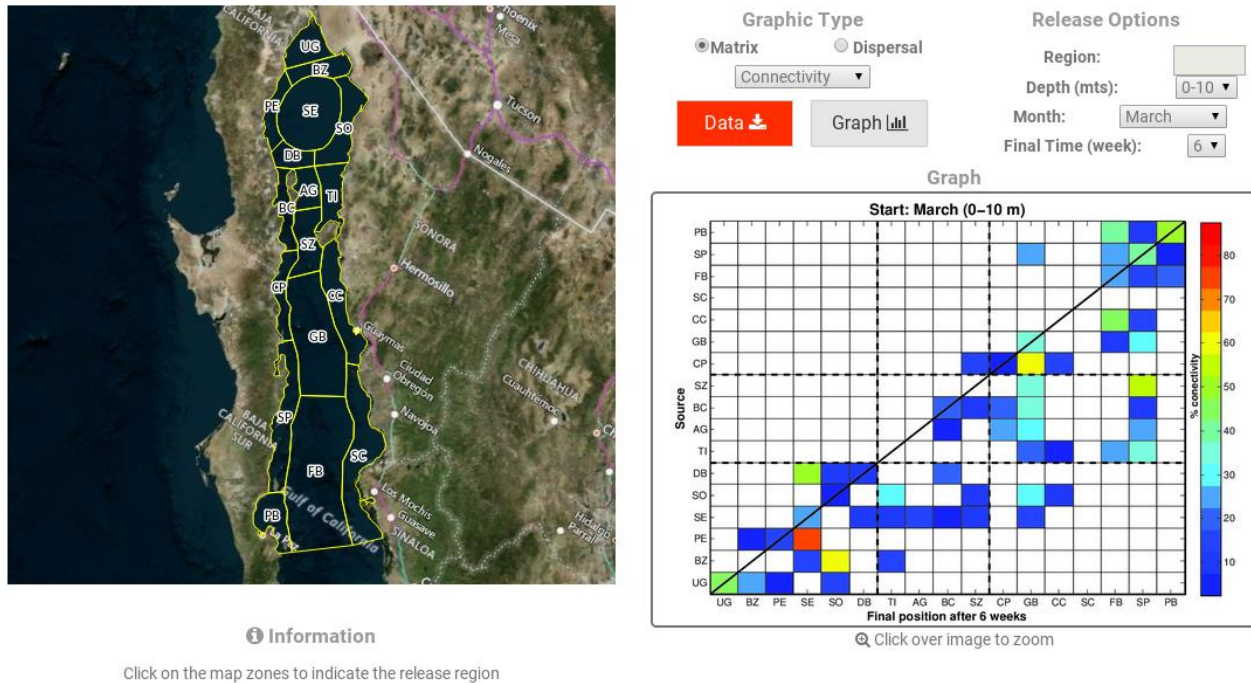


**Figure 2.** Example of a connectivity matrix. The release was completed in March at the first layer (0–10 m). In this case, the final time selected was the end of the sixth week.

the top central area of the webpage. Following, examples of both types of figures are described.

**a) Matrix**

For this graph, the matrix type must be selected: connectivity, mean depth or standard deviation; the

option is found at the top central part of the page. The release options are found at the top right, in which the user selects the depth (1 to 12 layers), the month (1 to 12 months) and the final visualization time (2, 4, 6 or 8 weeks). For example, Fig. 2 shows a connectivity matrix for March, releasing particles at a depth range of



**i** Information  
 Central Peninsular Region (CP)  
 Maximum number of layers: 11

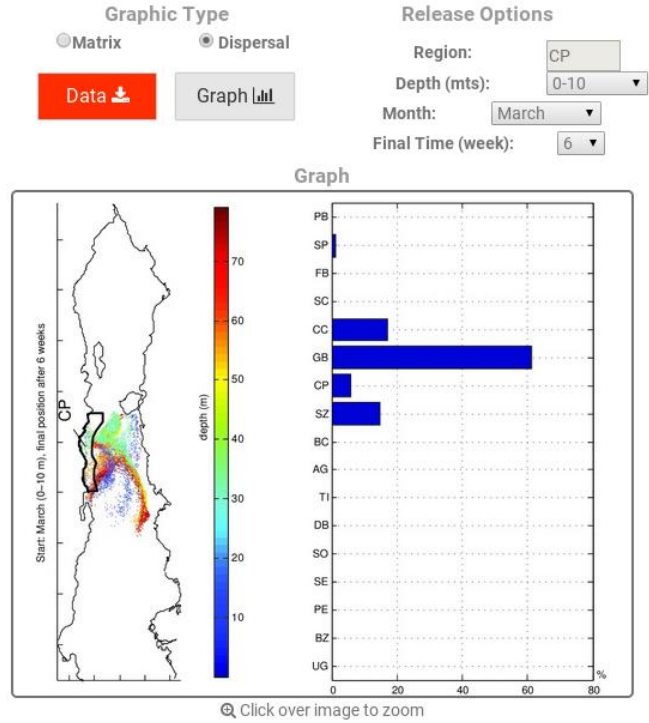
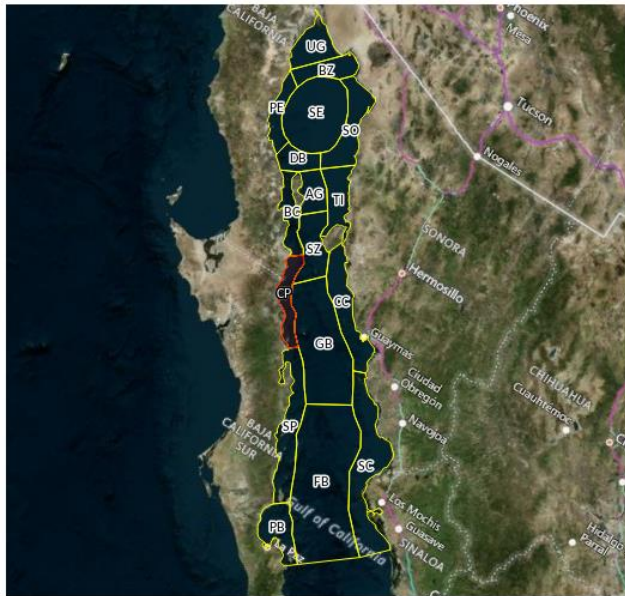


**Figure 3.** Example of a particle’s final position map and its corresponding histogram. The release was performed in the Central Peninsular Region (CP) in March at the first layer (0–10 m). In this case, the final time selected was the end of the sixth week.



**i** Information  
 Central Peninsular Region (CP)  
 Maximum number of layers: 11

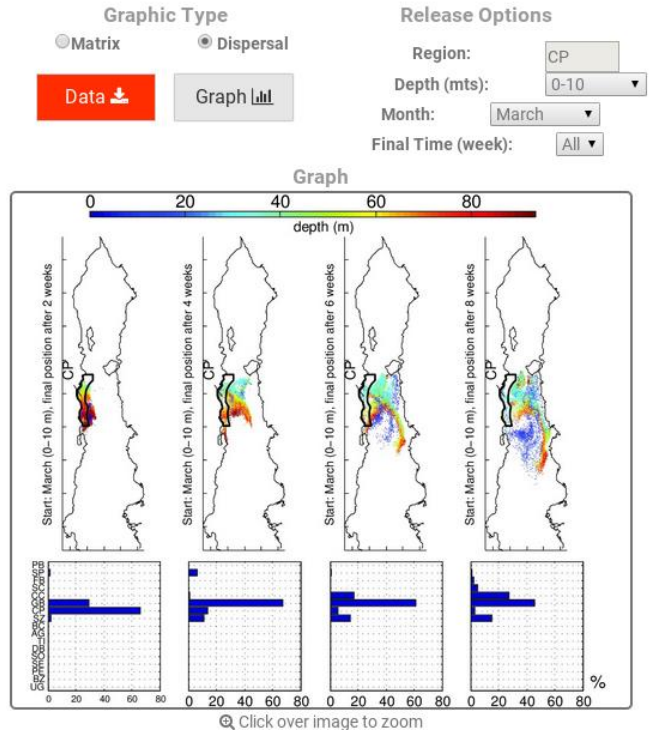


**Figure 4.** Example of a particle’s final position map and its corresponding histogram. The release was done in the Central Peninsular Region (CP) in March at the first layer (0–10 m). In this case, the option “All” was selected, displaying the four different final periods.

0–10 m and displaying the results for the sixth week after release. In contrast, Fig. 2 shows that the particles released in the Central Peninsular Region (CP) moved towards the Sills Zone (SZ), Guaymas Basin (GB) and Central Continental Region (CC), and a small percentage of the particles are found in the same sector in which they were released. Similarly, north of Tiburón Island (TI), six weeks after release, the particles moved towards the regions of GB, CC, Farallón Basin (FB) and the South Continental Region (SC).

The data for each connectivity, mean depth and standard deviation matrix may be downloaded by selecting the option “Data” located in the top center of the page. The format of the data is the same as that of the figure, that is, the horizontal axis represents the particle arrival location, and the vertical axis represents release areas.

### b) Dispersion

First, a release area must be selected; this is accomplished using the map located at the upper left of the page. This map shows the 17 regions into which the GC was divided, each with its associated acronym. The results are shown for the different depths of the GC and for the 12 months of the year. However, in the case of a particle’s final position, there are two options for displaying the results: specific, by selecting 2, 4, 6 and 8 weeks; and general, by selecting “all”, whereby all four results are displayed in a single image. Finally, in the lower left of the page there is an option for information, which provides the full name and number of layers of the area selected.

Figures 3 and 4 show examples of a specific map and a general map, respectively, of the final position of the particles and their corresponding histogram. This provides a visual representation of the steps described previously. It is important to note that the dispersion maps complement the matrix analysis.

Figure 3 shows the position of the particles six weeks after being released in the CP, which more precisely presents the particles’ paths, as well as depths at which they are located. In this case, the majority of the particles are found at depths greater than 40 m and predominantly moved in the direction of the GB sector. Fig. 4 depicts the four periods, permitting the trajectory of the particles to be inferred. In this case, at the end of the eighth week, a higher percentage of the particles released moved towards the east of the CP, CC and GB sectors. It was also observed that in the second region, the majority of the particles were located at depths >50 m; however, in the following weeks, most of these particles were located at depths <60 m.

Finally, it is possible to download the data from each map depicting the particles’ final positions by selecting the option “Data” located in the upper center of the page. The format of this document is presented in three columns (longitude, latitude, depth). The heading of the first row provides the Julian hour of the final positions, that is, the second, fourth, sixth and eighth weeks correspond to the hours 336, 672, 1008 and 1344, respectively. The remaining rows provide the positions of each particle.

## FINAL CONSIDERATIONS

The interactive online webpage developed in this study presents the three-dimensional connectivity results among 17 areas of the GC and the spatial distribution of particles released from each of the areas. These results were realized based on the advection of particles obtained from a 12-layer three-dimensional numerical model that was validated with respect to the primary circulation characteristics of the GC. The associated temporal scales are limited to model forcing, which correspond to the seasonal variations in tides; therefore, fluctuations in other frequencies are not considered for the model used in this interactive webpage. The results presented here are qualitative and should not be used as a key tool for decision making. However, the results offer an approximation of the connectivity and dispersion patterns in the GC, which may help in the understanding of dispersion patterns for marine organism larvae as well as contaminants.

## ACKNOWLEDGEMENTS

This study is part of the Masters of Science thesis of CMC, who was supported by a CONACyT scholarship. Financial support is part of the regular budget of the CICESE and of project CONACyT No. 44055.

## REFERENCES

- Beier, E. 1997. A numerical investigation of the annual variability in the Gulf of California. *J. Phys. Oceanogr.*, 27(5): 615-632.
- Calderon-Aguilera, L.E., S.G. Marinone & E.A. Aragón-Noriega. 2003 Influence of oceanographic processes on the early life stages of the blue shrimp (*Litopenaeus stylirostris*) in the Upper Gulf of California. *J. Mar. Syst.*, 39: 117-128.
- Carrillo, L., M.F. Lavín & E. Palacios-Hernández. 2002. Seasonal evolution of the geostrophic circulation in the northern Gulf of California. *Estuar. Coast. Shelf Sci.*, 54: 157-173.

- Cudney-Bueno, R., M.F. Lavín, S.G. Marinone, P.T. Raimondi & W.W. Shaw. 2009. Rapid effects of marine reserves via larval dispersal. *PLoS ONE*, 4(1): 1-7.
- Lavín, M.F., R. Durazo, E. Palacios, M.L. Argote & L. Carrillo. 1997. Lagrangian observations of the circulation in the northern Gulf of California. *J. Phys. Oceanogr.*, 27: 2298-2305.
- López, M., J. Candela & M.L. Argote. 2006. Why does the Ballenas Channel have the coldest SST in the Gulf of California?. *Geophys. Res. Lett.*, 33: 1-5.
- Marinone, S.G. 2003. A three-dimensional model of the mean and seasonal circulation of the Gulf of California. *J. Geophys. Res.*, 108(C10): 3325.
- Marinone, S.G. 2006. A numerical simulation of the two- and three-dimensional Lagrangian circulation in the northern Gulf of California. *Estuar. Coast. Shelf Sci.*, 68: 93-100.
- Marinone, S.G. 2008. On the three-dimensional numerical modeling of the deep circulation around Ángel de la Guarda Island in the Gulf of California. *Estuar. Coast. Shelf Sci.*, 80: 430-434.
- Marinone, S.G. & M.F. Lavín. 2005. Tidal current ellipses in a three-dimensional baroclinic numerical model of the Gulf of California. *Estuar. Coast. Shelf Sci.*, 64: 519-530.
- Marinone, S.G., M.J. Ulloa, A. Parés-Sierra, M.F. Lavín & R. Cudney-Bueno. 2008. Connectivity in the northern Gulf of California from particle tracking in a three-dimensional numerical model. *J. Mar. Syst.*, 71: 149-158.
- Montaño, C.C. 2015. Conectividad tridimensional durante verano en el norte del Golfo de California. Tesis Maestría en Ciencias, Centro de Investigación Científica y de Educación Superior de Ensenada, Baja California, 60 pp.
- Munguia-Vega, A., A. Jackson, S.G. Marinone, B. Erisman, M. Moreno-Baez, A. Girón-Nava, T. Pfister, O. Aburto-Oropeza & J. Torre. 2014. Asymmetric connectivity of spawning aggregations of a commercially important marine fish using a multidisciplinary approach. *Peer J*. 2:e511. Doi:10.7717/peerj.511.
- Proehl, J.A., D.R. Lynch, D.J. McGillicuddy & J.R. Ledwell. 2005. Modeling turbulent dispersion on the North Flank of Georges Bank using Lagrangian particle methods. *Cont. Shelf Res.*, 25: 875-900.
- Santiago-García, M.W., S.G. Marinone & O.U. Velasco-Fuentes. 2014. Three-dimensional connectivity in the Gulf of California based on a numerical model. *Prog. Oceanogr.*, 123: 64-73.
- Soto-Mardones, L., S.G. Marinone & A. Parés-Sierra. 1999. Time and spatial variability of sea surface temperature in the Gulf of California. *Cienc. Mar.*, 25: 1-30.
- Ripa, P. 1990. Seasonal circulation in the Gulf of California. *Ann. Geophys.*, 8: 559-564.
- Visser, A.W. 1997. Using random walk models to simulate the vertical distribution of particles in a turbulent water column. *Mar. Ecol. Prog. Ser.*, 158: 275-281.

*Received: 20 December 2015; Accepted: 27 December 2016*